High-spin states in ^{179}Au: Spectroscopy of shape-driving orbitals beyond the neutron midshell

W. F. Mueller,[1] W. Reviol,[2,3] M. P. Carpenter,[4] R. V. F. Janssens,[4] F. G. Kondev,[4,5] K. Abu Saleem,[4] I. Ahmad,[4] H. Amro,[4,6,*] C. R. Bingham,[2] J. Caggiano,[4,*] C. N. Davids,[4] D. Hartley,[2,†] A. Heinz,[4,*] B. Herskind,[7] D. Jenkins,[8] T. L. Khoo,[4] T. Lauritsen,[4] W. C. Ma,[6] J. Ressler,[4,9,*] L. L. Riedinger,[2] D. G. Sarantites,[3] D. Seweryniak,[4] S. Siem,[4,10] A. A. Sonzogni,[4,‡] J. Uusitalo,[4,§] P. G. Varmette,[5] I. Wiedenhöver,[4,‖] and R. Wadsworth[8]

[1]*The National Superconducting Cyclotron Laboratory, Michigan State University, East Lansing, Michigan 48824-1321, USA*
[2]*Department of Physics, University of Tennessee, Knoxville, Tennessee 37996, USA*
[3]*Department of Chemistry, Washington University, St. Louis, Missouri 63130, USA*
[4]*Physics Division, Argonne National Laboratory, Argonne, Illinois 60439, USA*
[5]*Nuclear Engineering Division, Argonne National Laboratory, Argonne, Illinois 60439, USA*
[6]*Department of Physics, Mississippi State University, Mississippi State, Mississippi 39762, USA*
[7]*The Niels Bohr Institute, DK-2100, Copenhagen, Denmark*
[8]*Department of Physics, University of York, Heslington, York YO1 5DD, United Kingdom*
[9]*Department of Chemistry, University of Maryland, College Park, Maryland 20742, USA*
[10]*Department of Physics, University of Oslo, N-0316, Oslo, Norway*

(Received 2 February 2004; published 15 June 2004)

Multiple band structures in ^{179}Au are established from γ-ray spectroscopic measurements with Gammasphere at the Argonne Fragment Mass Analyzer. The yrast band, based on the $13/2^+$ proton, confirms the predicted drop in excitation energy of the prolate deformed band head as compared to the heavier isotopes. The implications for the prolate energy minimum in odd-mass Au nuclei beyond the neutron $i_{13/2}$ midshell ($N<102$) are discussed.

DOI: 10.1103/PhysRevC.69.064315 PACS number(s): 21.10.Re, 27.70.+q

I. INTRODUCTION

The mercury-lead region below mass $A=190$ has been topical for many years. Located near a magic shell ($Z=82$), the nuclei involved exhibit a remarkable number of different shapes: spherical, oblate, and prolate deformed. Moreover, certain shapes are coexisting within a limited range of excitation energy in a given nucleus. Of particlar interest is the structure of the prolate excitation associated with a deformation $\beta_2 \sim 0.25$. This structure found, for example, in most of the Hg nuclei is attributed to $4p$-$4h$ excitations across the shell closure that involves $i_{13/2}$, $h_{9/2}$, and $f_{7/2}$ intruder orbitals with a low Ω quantum number [1]. Its intruder nature has been established in both in-beam studies and decay work by delineating the energy of the prolate structure as a function of neutron number at and beyond the neutron $i_{13/2}$ midshell ($N=103$). Specifically, the prolate structure in the mercury isotopes is observed to minimize in energy at $N=103$ [2]. It rises rapidly with respect to the less deformed oblate states beyond midshell [3,4]. While the general picture is settled, more experimental information is necessary to eludicate the contributions by the intruder orbitals to the exact structure of the prolate shape. In this context, new data for gold and thallium nuclei are desirable. This implies that an analogous prolate configuration is responsible for the yrast bands in even-Z and odd-Z nuclei, an assumption that is justified by the similarity of the moments of inertia for all these bands.

Recently, the behavior below midshell of the prolate states in the isotopic chains of thallium and lead nuclei has attracted considerable interest and spectroscopic studies of ^{183}Tl [5,6] and ^{182,184}Pb [7,8] nuclei have been carried out. In the case of ^{183}Tl ($N=102$), it was found that the prolate minimum, giving rise to a $\pi i_{13/2}$ structure, drops in excitation energy with respect to the heavier isotopes. It appears that the midshell behavior in this chain is different from that of the Hg nuclei. The results for the Pb nuclei, however, indicate the same behavior as for the Hg isotopes. Also recently, gold nuclei located significantly beyond midshell have been studied, viz., ^{177,175,173}Au [9] ($N=94,96,98$). Similar to the findings in the neighboring Hg isotones [3], the prolate states are present, but the oblate (or nearly spherical) levels dominate at low excitation energy. These level schemes mirror those of ^{185}Au [10] and ^{187}Au [11]. They are different from the level structures measured for the isotopes around midshell, ^{181,183}Au [12], where no oblate states were observed. Clearly, it is important to study ^{179}Au as the remaining odd-mass nucleus in the isotopic chain of gold. Additional interest is drawn to ^{179}Au in light of the recent results on ^{179}Hg [13], where three different shapes were shown to coexist, thus illustrating the strong shape competition in the mass region.

In order to follow the complete trend in odd-mass gold nuclei as one moves below the neutron midshell, two experi-

*Present address: Physics Department, Yale University, New Haven, CT 06520, USA.
†Present address: Physics Department, U.S. Naval Academy, Annapolis, MD 21402, USA.
‡Present address: National Nuclear Data Center, Brookhaven National Laboratory, Upton, NY 11973, USA.
§Present address: Department of Physics, University of Jyväskylä, Finland.
‖Present address: Department of Physics, Florida State University, Tallahassee, FL 32306, USA.

ments were performed in part to study the high-spin states in ^{179}Au. The experiments have been carried out with Gammasphere [14] at the Argonne Fragment Mass Analyzer [15]. The ^{179}Au nucleus, as other very proton-rich nuclei in the mass region, is difficult to study because the fusion-evaporation cross section is small compared to the fission yield in the decay of the compound system, and because the evaporation branch is fragmented into neutron and charged-particle channels. Hence, γ-ray spectroscopic methods can be combined with a "tagging" technique to select the evaporation residues of interest. The preferable technique is recoil-decay tagging (RDT) [16], which has been very successful when used to study nuclei decaying preferably by α (or proton) emission with a half-life in the seconds range (see, e.g., Refs. [3,4,9]). For the ground-state α emitter ^{179}Au with a half-life $t_{1/2}=7.1$ s, a branching ratio $b_\alpha \sim 20\%$ [17], and an α-decay energy $E_\alpha=5.85$ MeV, the RDT technique is quite suitable.

II. EXPERIMENTS AND DATA ANALYSIS

The results for ^{179}Au presented hereafter were obtained in two separate experiments using fusion-evaporation reactions with different projectile-target combinations. Both experiments were performed at the Argonne Tandem Linac Accelerator System (ATLAS), with the same experimental setup. The target was located at the center of the Gammasphere array, which contained at the time of the experiments 97 large-volume Ge detectors, all surrounded by BGO Compton suppressor shields, and four low-energy spectrometers (LEPS). The reaction products were allowed to recoil through the fragment mass analyzer (FMA) where they were separated from the large background of primary beam and fission fragments and dispersed at the focal plane according to their mass-to-charge ratio. The FMA was tuned such that typically three charge states of the central ion were within the acceptance of the device. The focal plane detector was a position-sensitive parallel-grid avalanche counter (PGAC) operated at a gas pressure of about 3 torr. On emerging from the PGAC, the recoils were implanted into a 60 μm thick double-sided silicon strip detector (DSSD) with 40×40 quasipixels.

With this setup, the γ rays from the target could be correlated first with residues detected in both the PGAC and the DSSD and, second, with the α decay following an implantation. The latter correlation method constitutes the already mentioned RDT technique. The data written to tape contained the following information: the energies and times (relative to the rf pulse of the Linac) of prompt γ rays detected at the target, the position and energy loss signals from the PGAC, the time of arrival of the particle at the PGAC relative to the prompt γ-ray flash, the energy deposited in the DSSD by the implant and the pixel that fired, the time-of-flight of the implanted particle between PGAC and DSSD, the energy of the α (or proton) decay of the implanted particle, and the absolute time of the event recorded by the so-called μs clock. As event trigger, it was required that at least two γ rays and a recoil detected in the PGAC were in concidence or that a DSSD event occurred (implant or decay).

In the first experiment a 340 MeV ^{78}Kr beam was used with an isotopically enriched ($>90\%$) ^{104}Ru target. The target had a surface density of 0.38 mg/cm^2 and was supported by a thin (≈ 100 μg/cm$_2$) Au layer facing the incoming beam. In this measurement, a total of 1×10^6 recoil γ^n ($n \geqslant 2$) events were recorded. The identification of γ rays from ^{179}Au ($p2n$ channel) was complicated by the presence of a large isobaric contaminant, ^{179}Pt ($2pn$).

The second experiment was performed using the ^{90}Zr(^{90}Zr, $1p$)^{179}Au reaction at beam energies of 369 and 380 MeV. The enriched ^{90}Zr target had a surface density of 0.55 mg/cm^2. Approximately 4×10^8 recoil γ^n ($n \geqslant 2$) events were collected in this case. Unlike in the first experiment, ^{179}Pt was not produced (impossible with a ^{180}Hg compound nucleus). Rather, the primary isobaric competitor to ^{179}Au was ^{179}Hg; that subset of the data leads to the results of Ref. [9].

The statistics from the first experiment proved insufficient to conclusively correlate newly observed γ rays with the α decay of ^{179}Au. A similar problem with this data set occurred when performing the γ-ray angular correlation analysis described below. Sufficient statistics were, however, available in the second experiment. Hence, only the α-γ and γ-ray angular correlations from the second experiment were considered at the final stage of the analysis. The construction of the ^{179}Au level scheme was based on the $A=179$ recoil gated γ-ray coincidences from both experiments. The two separate data sets provided consistent results for the placement of all transitions.

All γ-ray coincidence analyses were facilitated by sorting the mass-gated or RDT-gated γ-ray data into E_γ-E_γ matrices after unpacking the triple and higher-fold coincidence events and correcting the γ-ray energies for Doppler shifts and detector efficiencies. In addition, a mass-gated E_γ-E_γ-E_γ cube was created, following an analog sorting procedure. For the subsequent analysis steps, the RADWARE software package [18] was used.

Prompt γ-ray transitions in ^{179}Au were identified by applying the RDT technique under the following conditions: a gate on the characteristic α line with $E_\alpha=5.85$ MeV, a time window for the α decay of 20 s corresponding to approximately 3 half-lives ($t_{1/2}=7.1$ s), and the requirement that the preceeding DSSD implant event corresponds to a $A=179$ residue. The resulting γ-ray spectrum is shown in Fig. 1.

In order to obtain multipolarity information for the newly observed transitions, an angular correlation analysis was performed. For this purpose, an empirical anisotropy ratio was derived from the γ-ray intensities obtained from a set of two angle-sorted E_γ-E_γ matrices with the following specifications. The intensity for a particular γ ray observed in a projection for the Ge detectors at 30° and 150° versus all other Ge detectors in the Gammasphere array [$I(30)$] was divided by the intensity obtained from a projection for the detectors at 90° versus all other detectors [$I(90)$]. From transitions of known multipolarity in neigboring nuclei, it was established that this [$I(30)/I(90)$] ratio is $\sim$1.3 for a γ ray of stretched $E2$ character, and $\sim$0.7 for a pure stretched dipole transition. The multipolarity assignment for each transition was restricted to dipole radiation (with stretched $M1$ and $E1$ tran-

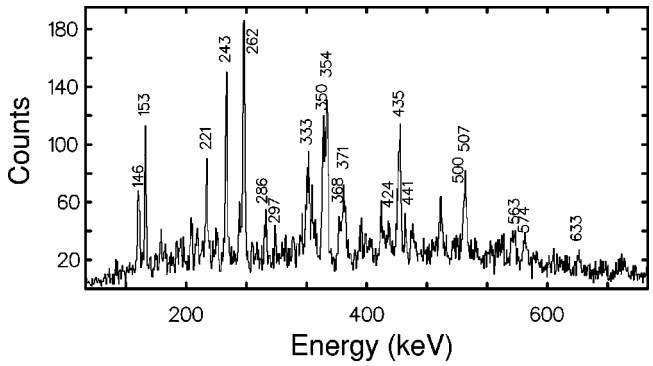

FIG. 1. Energy spectrum of γ rays generated by using the RDT technique. The γ rays shown are correlated with those mass 179 events from the ^{90}Zr+^{90}Zr reaction associated with a 5.85 MeV α peak and decay within 20 s. The transitions assigned to ^{179}Au are labeled by their energies in keV.

sitions being indistinguishable), electric quadrupole radiation $E2$, or radiation of the $E2+M1$ mixed type.

III. LEVEL SCHEME

The γ rays assigned to ^{179}Au are listed in Table I, together with their relative intensities, anisotropy ratios, and a labeling related to the level scheme (see below). The intensity of the strongest transition (E_γ=262 keV) is normalized to 100%. For the relative intensities measured in the second experiment, a distinction is made between the values obtained from mass-gated and RDT-gated γ-ray data. Thus, the relative γ-ray intensities listed in the column of Table I denoted by $I_{RDT}$are those observed in a correlation with ^{179}Au α decays as determined by fitting the peaks in a total projection of the RDT-gated E_γ-E_γ matrix.

Four rotational bands in ^{179}Au have been established primarily from the analysis of the recoil-mass selected γ-ray coincidence data. The new level scheme for ^{179}Au is shown in Fig. 2, where the bands are labeled 1 to 4 to ease their description. The γ-ray energies are those determined from the second experiment. Based on the favored α decay to the $5/2^-$ ground state of the daughter nucleus ^{175}Ir [19], the most likely spin and parity assignment to the band head of band 2 is $I=5/2^-$. The non-observation of any ground-state transition is most likely due to a small energy difference between the $9/2^-$ and $5/2^-$ states (cf. Fig. 2). However, as indicated in Fig. 1, the γ rays of the yrast and near-yrast states are found to be correlated with the α decay of the ground state.

The placement of in-band and interband transitions, which is also reported in Table I, is justified in the following paragraphs and a comment on the proposed spin and parity assignments is made at the end of the section. Band 1 is the yrast sequence of ^{179}Au and, as such, gathers the largest fraction of the total intensity. Figure 3 presents a representative coincidence spectrum generated by the sum of gates on the 153-, 262-, 354-, 435-, 507-, 574-, 633-, and 680-keV transitions. Clearly visible are the other band members with respective energies of 262, 354, 435, 507, 574, 633, and 680 keV. Their anisotropy ratios (cf. Table I) confirm the $E2$ character of these transitions. Additional weaker transitions for which anisotropy ratios could not be determined are also identified with band 1; these are at 739, 787, 822, and 840 keV. The decay out of the yrast band is rather complex and involves several other γ rays present in Fig. 3; specifically the 145-, 221-, 243-, 351-, and 372-keV lines. These transitions are observed in all coincidence spectra gated by in-band γ rays. Thus, they are associated with the decay out of band 1.

A spectrum gated by one of these transitions, the 221-keV γ ray, is given in Fig. 4(a). In addition to the transitions that form band 1, one also observes a strong 145-keV γ ray as well as transitions with respective energies of 333, 424, 500, and 560 keV. A careful analysis of their coincidence relationships shows that this set of γ rays forms a cascade labeled band 3 in Fig. 2. The 146-keV line, on the other hand, is proposed to be a linking transition between bands 1 and 3.

When gating on the 243-keV transition [Fig. 4(b)] one finds that its coincidence relationships with the prominent transitions of band 1 (cf. Fig. 3) are confirmed. In addition, a new set of γ rays with the respective energies of 350, 432, and 505 keV is observed. These are proposed to form together with the 243-keV line another band labeled 2. This band is assigned to ^{179}Au with great confidence, despite the fact that the 243-keV transition is part of a doublet with the other component being a transition in ^{179}Hg [13]. Band 1 is also observed to decay into band 2 by a 145-keV transition.

It should be noticed that band 1 decays to both bands 2 and 3 by transitions with similar energies of 145 and 146 keV, respectively. Support for these details of the level scheme is shown in Fig. 5. Its two panels show the spectrum from a double gate in the E_γ-E_γ-E_γ cube discussed in Sec. II on the 243- and 153-keV lines and, for comparison, similar gates on the 221- and 153-keV γ rays in panels (a) and (b), respectively. A 145-keV transition is clearly present in both spectra; however, careful inspection shows that there is an approximate one-channel shift between the two peaks. This corresponds to a $\approx$0.5-keV energy difference between these two transitions. Thus, the second excited states in bands 2 and 3 differ by only $\approx$0.5 keV

The presence of a fourth rotational band in ^{179}Au is documented by Fig. 4(c), which presents the coincidence gate on the 286-keV γ ray, a transition at the bottom of this sequence. The other in-band transitions have respective energies of 368, 441, 508, and 563 keV. A weak 192-keV γ ray is tentatively assigned to ^{179}Au, and could correspond to the lowest in-band transition. Also present in the coincidence spectrum of Fig. 4(c) is a prominent 297-keV transition. The angular correlation analysis shows that this 297-keV γ ray is most likely a dipole transition (see Table I). It is reasonable to view this γ ray as a decay-out transition for this band. A second decay-out branch from band 4 establishes a link to band 2 via a 340-keV γ ray. This transition can also be seen in Fig. 4(b), where, in addition, the 367- and 441-keV lines from band 4 are readily observed. The 297-keV transition is assumed to decay to the lowest level of band 2 on the basis of the following energy-sum consideration: the 297-keV and 286-keV γ rays sum up to the same value as the 243- and 340-keV transitions do.

TABLE I. Band assignments, energies, relative intensities, and anisotropy ratios for γ rays assigned to ^{179}Au. The typical uncertainties for the γ-ray energies are ±0.5 keV. The results from both experiments are reported (see text). The values χ and ξ are proportionality constants for the two 145-keV and two 350-keV transitions, respectively, that are unresolvable in RDT data.

	Experiment 1 ^{78}Kr(^{104}Ru, $1p2n$)		Experiment 2 ^{90}Zr(^{104}Zr, $1p$)			
Band	Energy	I_γ	Energy	I_γ	$\chi \times I_{RDT}$	$I(30)/I(90)$
$1 \rightarrow 2$	144.8	14.2 (1.5)	145.2	18.5 (1.1)	$\chi \times 31.7$ (2.5)	1.00 (0.06)
$1 \rightarrow 3$	145.4	21.3 (2.0)	145.7	29.5 (1.7)	$(1-\chi) \times 31.7$ (2.5)	[a]
$1 \rightarrow 1b$	349.9	33.6 (3.5)	350.5	39.5 (2.5)	$\xi \times 63.7$ (4.3)	1.09 (0.05)
$1 \rightarrow 1b$	370.5	22.1 (2.5)	371.5	20.1 (1.4)	36.9 (3.2)	1.43 (0.06)
1	152.7	48.6 (3.4)	153.1	47.6 (2.4)	39.8 (2.8)	1.20 (0.06)
1	261.7	100.0 (4.5)	262.1	100.0 (3.7)	100.0 (4.3)	1.31 (0.04)
1	353.6	76.9 (3.5)	354.1	88.3 (3.1)	78.1 (4.4)	1.39 (0.05)
1	434.2	57.1 (2.6)	434.6	66.6 (2.4)	64.5 (6.3)	1.40 (0.05)
1	507.0	37.7 (2.0)	507.2	40.1 (1.6)	44.3 (3.5)	1.08 (0.05)
1	573.3	23.3 (1.5)	573.7	21.4 (1.0)	13.8 (2.5)	1.52 (0.15)
1	632.7	8.2 (0.9)	633.2	7.3 (0.6)	9.3 (2.1)	1.46 (0.21)
1	679.3	4.5 (0.7)	680.4	3.5 (0.4)	9.4 (1.9)	1.14 (0.20)
1			738.7	<2%		
1			787.3	<2%		
1			822	<1%		
1			840	<1%		
2	242.4		242.7		69.0 (3.7)	1.24 (0.04)
2	350.0	32.6 (2.9)	350.4	39.9 (2.2)	$(1-\xi) \times 63.7$ (4.3)	[b]
2	431.2	24.3 (2.1)	431.9	26.8 (1.5)	14.0 (5.7)	1.21 (0.20)
2	505.8	18.9 (1.9)	505.4	20.4 (1.3)		[c]
3	220.7		220.9		39.5 (2.9)	1.27 (0.08)
3	332.2	13.5 (1.9)	332.7	15.7 (1.4)	39.9 (6.0)	1.26 (0.06)
3	423.4	13.7 (1.5)	423.7	14.1 (1.0)	16.0 (2.6)	1.29 (0.08)
3	500.0	9.4 (1.1)	500.2	10.2 (0.8)		1.84 (0.22)
3	559.1	3.5 (0.8)	559.7	4.0 (0.5)		
$4 \rightarrow 2$	296.7	11.4 (1.5)	297.1	9.4 (0.9)	7.5 (2.1)	0.66 (0.13)
$4 \rightarrow 2$	340.0	4.7 (0.9)	340.5	2.2 (0.5)		0.91 (0.41)
4			192.0	<2%		
4	285.9	12.6 (1.5)	286.2	10.8 (0.9)	16.2 (2.3)	1.06 (0.14)
4	367.5	18.0 (4.8)	367.8	18.9 (1.2)	20.7 (2.8)	1.11 (0.12)
4	440.5	13.5 (9.6)	441.2	14.9 (1.0)	10.6 (2.5)	1.11 (0.16)
4	507.2	10.3 (26.5)	507.5	13.5 (0.9)		[c]
4	562.2	5.8 (29.0)	562.7	7.7 (0.7)		1.51 (0.26)

[a]The 145.2- and 145.7-keV transitions are not resolved.
[b]The 350.5- and 350.4-keV transitions are not resolved.
[c]The 507.5-, 505.4-, and 507.2-keV transistions are not resolved.

A level at the excitation energy of $(x+17$ keV) (noted at band 1b in Fig. 2) is established by the 351- and 371-keV transitions with the latter decaying out of the bottom of band 1. The 351-keV line is also a doublet with a transition in band 2. The angular correlation results for these two γ rays indicate that they are of quadrupole type; however, the uncertainty on the angular correlation of the 351-keV transition is rather large. It can be ruled out that the 242- and 350-keV γ rays appear in cascade below the lowest level of band 1 by the analysis of double-gated coincidences. Neither this 350-keV line nor the371-keV γ ray show coincidences with transitions other than those of band 1. There are two possible options for the placement of these γ rays. The first implies that these decay from the lowest observed level in band 1 to two distinct states separated by 17 keV. The second option is that they decay to the same state, but the 350-keV transition is from an unobserved level in band 1 located 17 keV below the lowest state that we observe. It is not possible to differ-

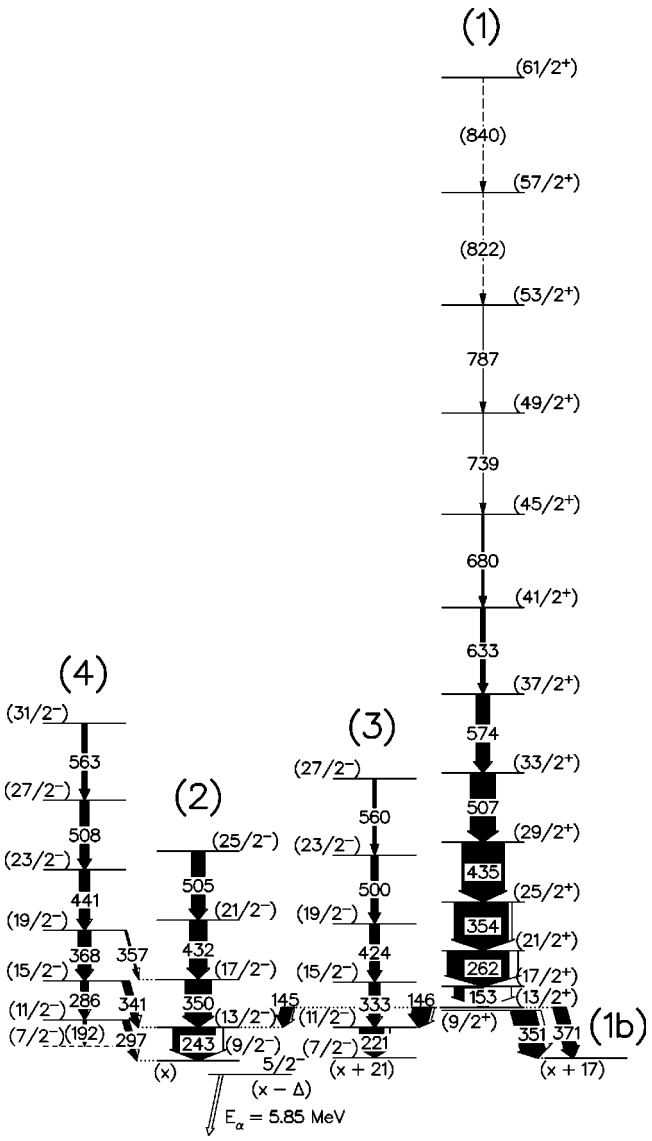

FIG. 2. Level scheme for ^{179}Au deduced from this work. The location of the $9/2^-$ state with respect to the ground state remains uncertain as indicated by x. In addition the known α-decaying $5/2^-$ state is denoted at an unknown energy (Δ) below the $9/2^-$ level.

entiate between these options based solely on the experimental observations; however, a preference for option 2 (as indicated in Fig. 2) is found on the basis of a comparison with the level scheme for ^{177}Au [9]—see Sec. IV A for further justification. By the same token, transitions similar to the 350- and 371-keV γ rays in ^{179}Au have not been observed in the heavier odd-mass Au nuclei.

Since there is no known transition from the observed level to the ^{179}Au ground state, the assignments for the band-head states rest on systematic comparisons with band structures in the heavier odd-mass Au nuclei. To facilitate such comparisons, the low-spin structures of ^{179}Au and ^{181}Au are shown in Fig. 6 where the level scheme for ^{181}Au serves as a representative for the heavier isotopes. There is an obvious similarity between the yrast band in ^{179}Au and the corresponding structures in ^{181}Au, ^{183}Au, and ^{185}Au, the latter being based on a $13/2^+$ state. Therefore, the state at an $(x+387)$-keV

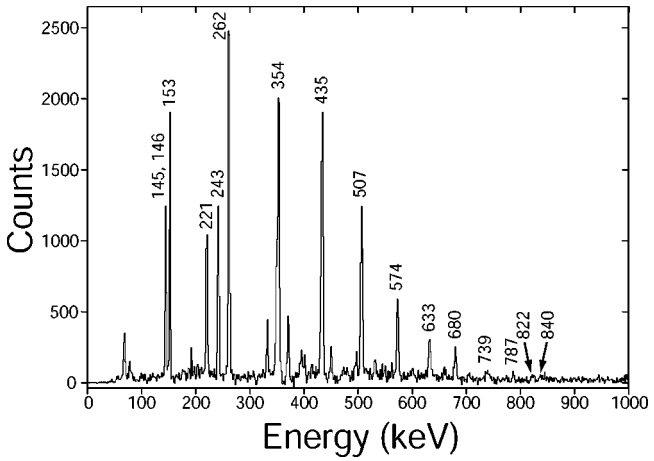

FIG. 3. Representative $A=179$ gated γ-ray coincidence spectrum from the ^{90}Zr(^{90}Zr,$1p$)^{179}Au experiment (no RDT gating). The spectrum is generated from the sum of 153-, 262-, 354-, 435-, 507-, 574-, 633-, and 680-keV gated spectra.

excitation energy in ^{179}Au is assigned a spin and parity of $13/2^+$. Furthermore, the positive-parity bands in ^{181}Au, ^{183}Au, and ^{185}Au are observed to decay out of the $13/2^+$ state to $13/2^-$ and $11/2^-$ levels in lower-lying band structures. The states near the bottom of bands 2 and 3 are assigned the same spins, by analogy.

IV. DISCUSSION

The primary reason for studying the high-spin structure of ^{179}Au is to understand the trend of the prolate proton intruder bands ($\pi i_{13/2}$, $\pi h_{9/2}$, and $\pi f_{7/2}$) in nuclei below the $N=103$ neutron midshell. The motivation is a twofold one: (i) to study the excitation energies of these structures relative to each other, and (ii) to learn about deformation trends as a function of mass number.

A. Configuration assignments

In $175 \leqslant A \leqslant 187$ odd Au isotopes, the yrast sequence at moderate spins (e.g., $17/2\hbar$ to $53/2\hbar$) is associated with the $\pi i_{13/2}$ intruder band [9–12]. The low-K, prolate character of this sequence (as expected for orbitals near the bottom of a shell) is indicated by its large signature splitting (i.e., only one signature is observed). In those nuclei, this band is observed to end at the $13/2^+$ band head, and the decay out of this level feeds $13/2^-$ and $11/2^-$ states in $\pi h_{9/2}$ and $\pi f_{7/2}$ configurations. The same appears to apply for ^{179}Au.

As discussed in the preceding section, it is likely that the 350- and 371-keV γ rays feed separate states, or a single state from separate levels in band 1. It is possible that Coriolis coupling of the valence proton to the core is sufficiently weakened that the $9/2^+$ state of the $\pi i_{13/2}$ band drops lower in energy than the $13/2^+$ level. If this is indeed the case, it is likely that the 371-keV γ ray decays directly from the $13/2^+$ state of band 1, while the 351-keV transition decays from the $9/2^+$ level.

Below the $13/2^+$ state in ^{181}Au and heavier Au nuclei, the yrast levels are assigned to the favored signature (α

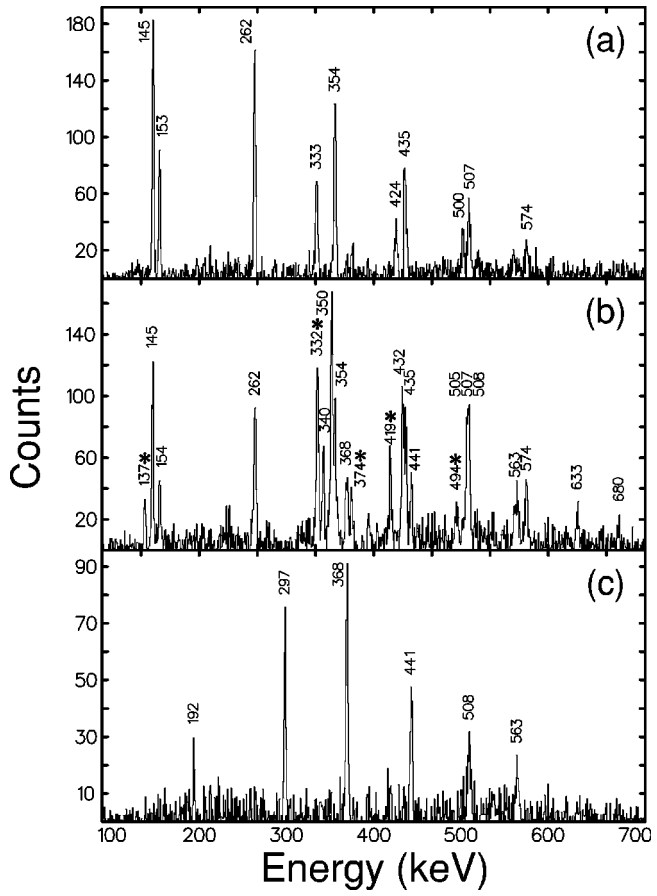

FIG. 4. Representative $A=179$ gated γ-ray coincidence spectra from the ^{90}Zr(^{90}Zr, $1p$)^{179}Au experiment (no RDT gating). As gating transitions γ rays with the respective energies of (a) 221 keV, (b) 243 keV, and (c) 286 keV are used. The γ rays in spectrum (b) marked by an asterisk are known contaminants from ^{179}Hg (cf. Ref. [13]).

$=+1/2$) of the $\pi h_{9/2}$ orbital. Similarly, band 2 in ^{179}Au is assigned to this configuration. Bands 3 and 4 can then be interpreted as associated with mixed configurations of the unfavored $\pi h_{9/2}$ and favored $\pi f_{7/2}$ orbitals.

In ^{187}Au [11], the ground state is attributed to a spherical $\pi s_{1/2}$ configuration, but prolate rotational bands are observed at low excitation energies ($\approx$100 KeV). In ^{185}Au, a prolate-deformed configuration becomes the ground state [10,20], and the next lighter isotopes, ^{181}Au and ^{183}Au, are observed to be prolate in their ground states as well [12].

The lowering in excitation energy of the prolate configurations is understood as being due primarily to the approach and crossing of the neutron midshell (^{185}Au has $N=104$). However, a second, more subtle, factor driving the deformation is the occupation of the valence proton in a deformation-driving intruder state. A calculation of single-particle states in a Woods-Saxon potential as a function of quadrupole deformation (β_2) is presented in Fig. 7. It can be seen that, at large deformations ($\beta_2 \sim 0.25$), a gap appears at $Z=78$. This gap occurs between intruding states originating from $h_{9/2}$, $f_{7/2}$, and $i_{13/2}$ spherical orbitals and the $s_{1/2}$, $d_{3/2}$, and $h_{11/2}$ in-shell states. When the intruder states are occupied, one would expect an enhancement of the deformation.

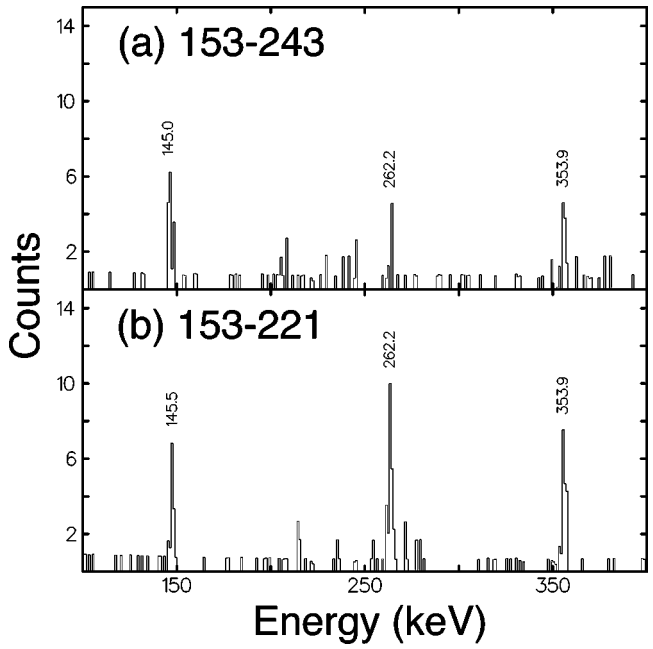

FIG. 5. Double-gated γ-ray spectra displayed around the energy of 145 keV. Panel (a) is a double gate on 153- and 221-keV γ rays, and panel (b) a double gate on the same 153-keV transition and the 243-keV peak.

This has been verified by a measurement of lifetimes in a selected case, ^{187}Au [21], where the Fermi level is far from the intruder state. However, this picture is also supported by lifetime measurements in neighboring $A \leqslant 181$ Ir nuclei [22,23] and by the recent lifetime measurement in ^{188}Pb [24]. Notice that the lack of lifetime information for $A<187$ Au nuclei is due in part to the experimental difficulty of carrying out such measurements (cf. Ref. [24]).

It is possible to make qualitative assessments of the deformation driving characteristics of intruder bands by the

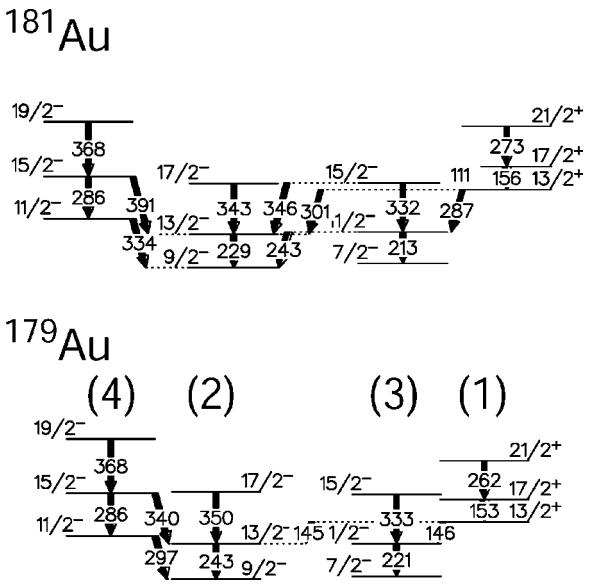

FIG. 6. Comparison of the low-spin level schemes for ^{179}Au (this work) and ^{181}Au [12]. The band structures of ^{179}Au are labeled as in Fig. 2.

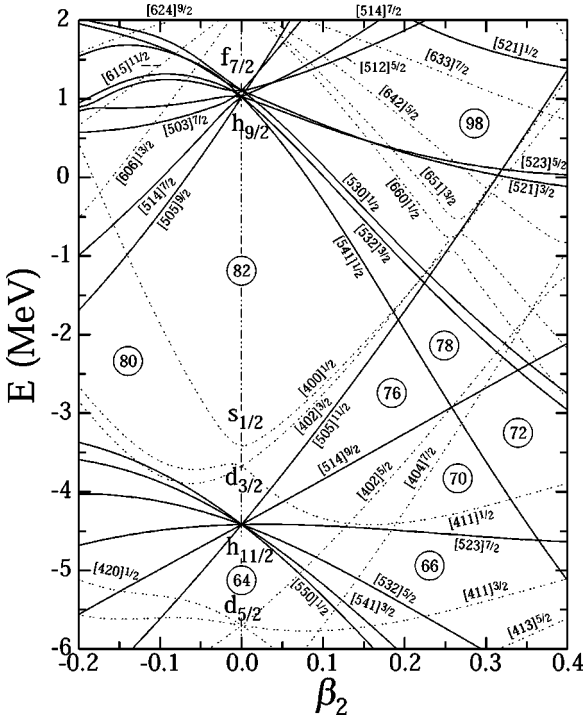

FIG. 7. Deformed single-particle level diagram around $Z=79$ calculated with a Woods-Saxon potential with $\beta_4=\gamma=0$.

investigation of other properties. Three of these properties are the relative excitation energy of intruder band heads, the delay in rotational frequency of quasiparticle band crossings, and differences in the moments of inertia of rotational bands. These three properties are discussed in the following sections.

B. Band-head energies

Systematic comparisons of band-head energies of excited states with respect to the ground states of the respective nuclei can be deceiving since the ground-state configuration can possibly change from one nucleus to the next. However, from the comparison of relative band-head energies, it is possible to gain insight into changes between specific configurations. Figure 8 shows such a comparison between the $\pi i_{13/2}$ and $\pi h_{9/2}$ band heads for Au nuclei with $N=98$ to 108. Also in this figure are the corresponding results of potential-energy surface calculations [12].

It can be seen that the band-head energy of the $\pi i_{13/2}$ orbital is dropping rather strongly with respect to the $\pi h_{9/2}$ configuration. This is expected if the deformation associated with the former orbital is larger than that associated with the latter and if in both cases the change of the deformation parameter as a function of N (as obtained from theoretical calculations) is about the same. This expectation is further substantiated in the paragraph below. However, it is interesting to note that even below the midshell, the $i_{13/2}-h_{9/2}$ energy difference continues to decrease. See Ref. [9] for further discussion of this point and its relation to shape driving effects in the Au nuclei.

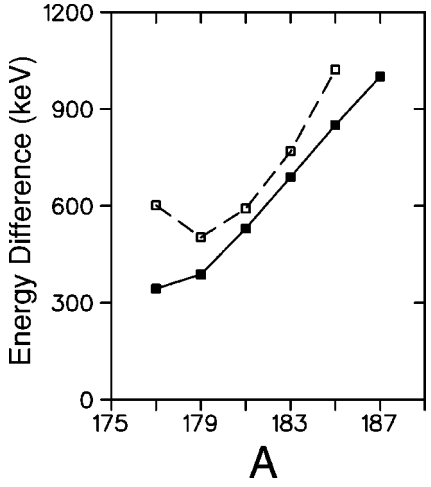

FIG. 8. Experimental (i.e., the energy difference between the lowest-energy $13/2^+$ and $9/2^-$ states) and theoretical energy differences between the $\pi i_{13/2}$ and $\pi h_{9/2}$ band heads in Au. The solid squares are the experimental energy differences, while the open symbols are theoretical values.

It was predicted from the calculations presented in Ref. [12] that the minimum energy difference between the $\pi i_{13/2}$ and $\pi h_{9/2}$ states should actually occur in ^{179}Au. The calculated β_2 parameters for the $\pi i_{13/2}$ $\frac{1}{2}$[660] band heads in odd-A ^{177}Au to ^{185}Au are 0.244, 0.246, 0.251, 0.254, and 0.250, respectively. By comparison, the $\pi h_{9/2}$ $\frac{1}{2}$[541] states have calculated deformations of 0.195, 0.215, 0.263, 0.226, and 0.223. As can be seen in the calculated $i_{13/2}$ systematics above, ^{183}Au ($N=104$) is predicted to have the largest deformation. This can also be seen in the calculated $h_{9/2}$ deformation, with the exception of ^{181}Au where the β_2 value does not seem to fit the systematic trend. It should be noted that the $h_{9/2}$ configuration is far from pure, and has significant interaction and mixing with the $\pi f_{7/2}$ configuration.

C. $(\nu i_{13/2})^2$ crossing frequency

Another factor that can be used to determine the relative deformation between various configurations is the frequency at which a pair of nucleons occupying a high-j orbital aligns. As deformation is known to be one of the factors influencing the alignment frequency [25], it has been shown that the alignment frequency of a $\nu i_{13/2}$ pair increases with quadrupole deformation [26]. In the case of nuclei around $N=104$, the $\nu i_{13/2}$ shell is about half filled, and it is the alignment of neutrons from this orbital that is the most commonly observed as the lowest frequency band crossing. The experimental situation in gold is complicated somewhat because it is believed that an $h_{9/2}$ proton alignment occurs at a similar frequency in the heavier Au nuclei [11].

The alignments, i, of the $\pi i_{13/2}$ bands in odd-A ^{179}Au, ^{181}Au, ^{183}Au, and ^{185}Au are plotted versus the rotational frequency in Fig. 9. Rather complicated up-bend structures are observed in the bands of both ^{183}Au [Fig. 9(c)] and ^{185}Au [Fig. 9(d)]. In these two nuclei the $(\pi h_{9/2})^2$ and $(\nu i_{13/2})^2$ crossings are thought to occur at similar frequencies [10,12]. While the precise rotational frequency of the $(\nu i_{13/2})^2$ cross-

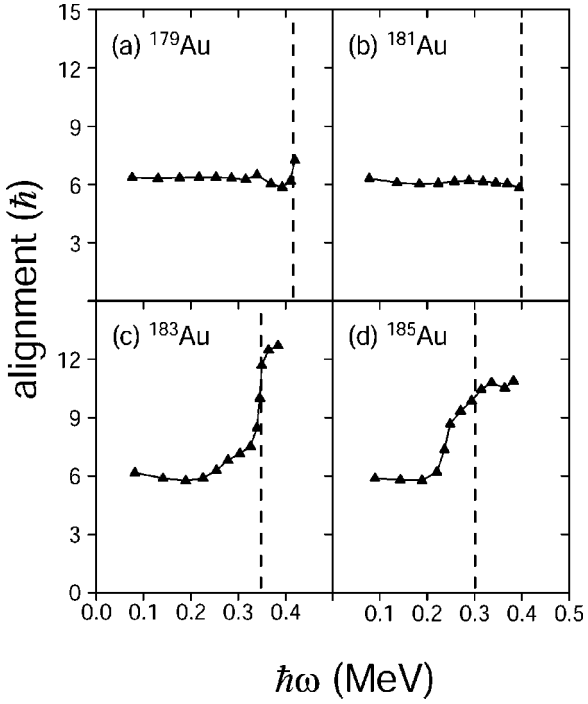

FIG. 9. Experimental rotational alignment plots for the $\pi i_{13/2}$ bands in (a) ^{179}Au, (b) ^{181}Au, (c) ^{183}Au, and (d) ^{185}Au. The vertical dashed lines indicate the estimated locations (or, in the case of ^{181}Au, the lower limit) of the $(\nu i_{13/2})^2$ band crossing in each of these nuclei. The alignment in all four panels are calculated relative to a Harris parameterization of the moment of intertia with values for $\mathcal{J}_0$ and $\mathcal{J}_1$ of 33.5 $\hbar^2$/MeV and 131 $\hbar^4$/MeV^3, respectively.

ing cannot be determined because of this, one can observe for ^{185}Au that the crossing does not occur higher than $\hbar\omega = 0.3$ MeV. Similarly for ^{133}Au, the crossing occurs at not greater than $\hbar\omega = 0.35$ MeV. This implies that the quadrupole deformation of the $\pi i_{13/2}$ band in ^{183}Au is more deformed than in ^{185}Au.

In Fig. 9(b), one observes that the characteristic crossing is much delayed in ^{181}Au in comparison to ^{183}Au and ^{185}Au, since it is not observed up to a frequency of 0.4 MeV. This indicates that the quadrupole deformation of the $\pi i_{13/2}$ band in ^{181}Au continues to increase past the $N = 104$ midshell. A similar delay is observed in the $\pi i_{13/2}$ band of ^{179}Au, where a possible band crossing is observed at about $\hbar\omega = 0.42$ MeV, indicating that the deformation of the $\pi i_{13/2}$ band may perhaps continue to increase even to $N = 100$. This result is perhaps in conflict with the deformations predicted by the theoretical calculations discussed in Sec. IV B. While not pictured in Fig. 9, one can see in Ref. [9] that also the crossing frequency in ^{177}Au appears to occur at a rotational frequency greater than 0.35 MeV.

D. Moments of inertia

The transition energies in the lower parts of the $\pi i_{13/2}$ bands decrease in energy from ^{187}Au to ^{177}Au. For example, the energies of the $21/2^+ \rightarrow 17/2^+$ transitions in ^{185}Au, ^{183}Au, ^{181}Au, ^{179}Au, and ^{177}Au are 287, 283, 273, 262, and 257 keV, respectively. The transition energy is related to the moment of inertia by the formula presented by Bohr and Mottelson [27]:

$$\mathcal{J}^{(1)} = [I_x^2(i) - I_x^2(f)]/[2E_\gamma(i \rightarrow f)], \tag{4.1}$$

where $I_x(i/f) = \sqrt{I(i/f)[I(i/f)+1] - K^2}$ and $E_\gamma(i \rightarrow f)$ is the transition energy from the initial state, i, to the final state, f. I is the angular momentum of the state and K is the angular momentum projection onto the axis of deformation.

Harris [28] showed that the moment of inertia of a rotational band can be parametrized as

$$\mathcal{J}^{(1)} = \frac{i}{\omega} + \mathcal{J}_0 + \mathcal{J}_1\omega^2, \tag{4.2}$$

where $\mathcal{J}_0$ and $\mathcal{J}_1$ are the static and frequency dependent parameters of the moment of inertia. The first term (i/ω) was not part of Harris's original expansion, but is added here to account for an initial alignment, i, in the case of an odd-A nucleus with a particular configuration.

By fitting the lower parts of the $\pi i_{13/2}$ bands in the odd-A Au nuclei one obtains the parameters i, $\mathcal{J}_0$, and $\mathcal{J}_1$ presented in Table II. From these fits it can be seen that the $\mathcal{J}_0$ parameter increases from ^{187}Au to ^{177}Au, while the $\mathcal{J}_1$ values decrease from ^{187}Au to ^{177}Au.

The moment of inertia is related to deformation by Migdal's relation [29], which can be written as

$$\mathcal{J}_{Migdal} = J_{rig}\left[1 - f\left(\frac{\delta\hbar\omega_0}{2\Delta}\right)\right], \tag{4.3}$$

where

TABLE II. Harris parameters (i, $\mathcal{J}_0$, and $\mathcal{J}_1$) obtained by fitting the $\pi i_{13/2}$ rotational bands, total pairing energies (Δ), and $\sqrt{\Delta^2\mathcal{J}_0}(\delta_\mathcal{J})$ for $N = 98-108$ odd-A Au isotopes.

N	i ($\hbar$)	$\mathcal{J}_0$ ($\hbar^2$/MeV)	$\mathcal{J}_1$ ($\hbar^4$/MeV^3)	Δ (MeV)	$\delta_\mathcal{J}$ (MeV$^{1/3}\hbar$)
98	5.09(10)	34.7(1.0)	209(7)	1.26(24)	7.4(2.0)
100	5.36(15)	33.5(1.4)	131(10)	1.20(20)	7.0(1.7)
102	5.43(27)	31.6(2.7)	136(18)	1.13(18)	6.4(1.5)
104	5.65(31)	25.5(3.0)	233(28)	1.09(19)	5.5(1.5)
106	5.49(33)	25.6(3.3)	264(22)	1.11(21)	5.6(1.7)
108	5.48(62)	22.4(6.2)	250(42)	1.08(23)	5.1(2.1)

$$f(x) \equiv \frac{\ln[x + (1+x^2)^{1/2}]}{x(1+x^2)^{1/2}}. \quad (4.4)$$

There, $\mathcal{J}_{rig}$ is defined as the rigid moment of intertia, δ is the deformation parameter from the deformed harmonic oscillator potential expressed in spherical coordinates, $\hbar\omega_0$ is the characteristic harmonic oscillator frequency, and Δ is the pairing energy-gap parameter.

Applying a Taylor series expansion to Eq. (4.4) around $x=0$ and taking only lowest order terms give the approximate relation

$$f(x) \approx 1 - \frac{2}{3}x^2. \quad (4.5)$$

Substituting Eq. (4.5) into Eq. (4.3), gives the following proportionality:

$$\mathcal{J}_{mig} \propto \left(\frac{\delta}{\Delta}\right)^2. \quad (4.6)$$

Thus, the moment of inertia is not only dependent on deformation, but also on proton and neutron pairing.

The pair gap for neutrons (Δ_n) and protons (Δ_p) can be determined from even-odd mass differences using Eqs. (2-92) and (2-93) in Ref. [30]. An average overall pairing energy is determined by combining the neutron and proton values:

$$\Delta = \sqrt{[\Delta_n^2 + (0.8\Delta_p)^2]/2}. \quad (4.7)$$

Note that only 80% of the proton pairing energy is assumed in order to simulate the effect of quantum-state blocking that the odd proton in Au will produce. The calculated average overall pair gap for the $^{177-187}$Au odd-A isotopes using binding-energy data from Ref. [31] is also given in Table II.

Presented in the last column of Table II is the value of $\sqrt{\Delta^2\mathcal{J}_0}(\delta_{\mathcal{J}})$, which was shown above [see Eq. (4.6)] to be proportional to quadrupole deformation. One observes in the table that $\delta_{\mathcal{J}}$ is relatively constant for $^{183-187}$Au isotopes, but for ^{181}Au, ^{179}Au, and ^{177}Au, $\delta_{\mathcal{J}}$ becomes increasingly larger. This provides a third observable indicating that the deformation of the $\pi i_{13/2}$ bands in odd-A Au nuclei continues beyond the $N=103$ midshell.

V. CONCLUSIONS

High-spin states in ^{179}Au have been observed for the first time. From this study, four rotational bands have been identified and these are associated with $\pi i_{13/2}$, $\pi h_{9/2}$, and $\pi f_{7/2}$ prolate deformed configurations.

From the comparison of the $\pi i_{13/2}$ band in ^{179}Au with previously observed $\pi i_{13/2}$ structures in heavier odd-A Au nuclei, it is possible to deduce that the deformation of the $\pi i_{13/2}$ configuration in ^{179}Au ($N=100$) is larger than that of the same configuration in the heavier Au nuclei, despite being beyond the neutron midshell. This deduction is made from the comparison of three observables: band-head energies, $\nu i_{13/2}$ crossing frequencies, and moments of inertia.

The deformation trend for the $\pi i_{13/2}$ structure has been compared with the theoretical predictions made in Ref. [12], and some disagreement between the information based on experimental observation and these theoretical results is found. While the reason for the increasing deformation in the $\pi i_{13/2}$ bands of ^{181}Au and ^{179}Au is not entirely understood, it is clear that the presense of the odd proton in the $i_{13/2}$ orbital must play a key role in the stabilization of the deformation of the light ($N<104$) Au nuclei.

ACKNOWLEDGMENTS

This work was supported in part by the U.S. Department of Energy under Contract No. W31-109-ENG-38 (ANL), and the U.S. National Science Foundation under Grant No. PHY-0110253. W.F.M. thanks W. Nazarewicz for illuminating discussions about the paramentrization of deformation from the moment of inertia.

[1] J. L. Wood, K. Heyde, W. Nazarewicz, M. Huyse, and P. Van Duppen, Phys. Rep. **215**, 101 (1992).
[2] G. D. Dracoulis, A. E. Stuchbery, A. O. Macchiavelli, C. W. Beausang, J. Burde, M. A. Deleplanque, R. H. Diamond, and F. S. Stephens, Phys. Lett. B **208**, 365 (1988).
[3] M. P. Carpenter *et al.*, Phys. Rev. Lett. **78**, 3650 (1997).
[4] M. Muikku *et al.*, Phys. Rev. C **58**, R3033 (1998).
[5] W. Reviol *et al.*, Phys. Rev. C **61**, 044310 (2000).
[6] M. Muikku *et al.*, Phys. Rev. C **64**, 044308 (2001).
[7] D. G. Jenkins *et al.*, Phys. Rev. C **62**, 021302(R) (2000).
[8] J. F. C. Cocks *et al.*, Eur. Phys. J. A **3**, 17 (1998).
[9] F. G. Kondev *et al.*, Phys. Lett. B **512**, 268 (2001).
[10] A. J. Larabee *et al.*, Phys. Lett. **169B**, 21 (1986).
[11] J. K. Johansson *et al.*, Phys. Rev. C **40**, 132 (1989).
[12] W. F. Mueller *et al.*, Phys. Rev. C **59**, 2009 (1999).
[13] F. G. Kondev *et al.*, Phys. Lett. B **528**, 221 (2002).
[14] I.-Y. Lee *et al.*, Nucl. Phys. **A520**, 641c (1990).
[15] C. N. Davids *et al.*, Nucl. Instrum. Methods Phys. Res. B **70**, 358 (1992).
[16] E. S. Paul *et al.*, Phys. Rev. C **51**, 78 (1995).
[17] E. S. Firestone and V. S. Shirley, *Table of Isotopes*, 8th ed. (Wiley, New York, 1996), Vol. II.
[18] D. C. Radford, Nucl. Instrum. Methods Phys. Res. A **361**, 297 (1995).
[19] A. O. Macchiavelli and E. Browne, Nucl. Data Sheets **69**, 903 (1993).
[20] K. Wallmeroth *et al.*, Phys. Rev. Lett. **58**, 1516 (1987).
[21] J. C. Walpe *et al.*, Acta Phys. Pol. B **26**, 279 (1995).
[22] R. Kaczarowski, U. Garg, A. Chaudhury, E. G. Funk, J. W. Mihelich, D. Frekers, R. V. F. Janssens, and T. L. Khoo, Phys. Rev. C **41**, 2069 (1990).
[23] D. Müller *et al.*, Phys. Lett. B **332**, 265 (1994).
[24] A. Dewald *et al.*, Phys. Rev. C **68**, 034314 (2003).
[25] W. Walús *et al.*, Phys. Scr. **34**, 710 (1986).

[26] H.-Q. Jin *et al.*, Phys. Rev. C **53**, 2106 (1996).
[27] A. Bohr and B. Mottelson, *Nuclear Structure* (Benjamin, Reading, MA, 1975), Vol. II.
[28] S. M. Harris, Phys. Rev. **13**, 663 (1964).
[29] A. B. Migdal, Nucl. Phys. **13**, 655 (1959).
[30] A. Bohr and B. Mottelson, *Nuclear Structure* (Benjamin, Reading, MA, 1969), Vol. I.
[31] G. Audi, A. H. Wapstra, and C. Thibault, Nucl. Phys. **A729**, 337 (2003).